Abstract

We consider interactions beyond the Standard Model, possibly stemming from a higher-order theory. We show how the parameters of these Non-Standard Interactions (NSI) can modify the oscillation probabilities and within which energy range we expect to discern this signal. We use data from and simulate event counts in two Cherenkov detectors: IceCube and DeepCore. Moreover, we generate data and simulate a proposed upgrade of the DeepCore detector: PINGU.

We obtain stringent bounds on the NSI parameters and compare those to previous results in literature. We show that PINGU is expected to narrow the bound further on $\epsilon_{\mu\tau}$, especially by considering a joint analysis with IceCube and DeepCore. Finally, we see that an anti-correlation between $\epsilon_{e\mu}$ and $\epsilon_{e\tau}$ at probability level was propagated down to event level, which we expect to be observable by PINGU.

Acknowledgements

The computations were enabled by resources provided by the Swedish National Infrastructure for Computing (SNIC) at HPC2N, Umeå University and NSC, Linköping University. The resources were partially funded by the Swedish Research Council through grant agreement no. 2018-05973

1 The Standard Model

In order to describe the three quantizable forces of nature, we gather the mediators of each force – the vector bosons – into local (gauge) symmetry groups. Each vector boson has one corresponding generator, the set of which constitutes the group. The strong charge is mediated by eight massless gluons, which correspond to the eight independent generators of $\mathrm{SU}(3)_C$. The weak charge is mediated by the three massive gauge bosons $W^{\pm}$ and Z, and the massless photon γ, which constitute the generators of $\mathrm{SU}(2)_L$ and $\mathrm{U}(1)_Y$.

The subscript of each group denotes by which mechanism that force is mediated. The gluons mediate the strong force through interactions of color, emphasized with subscript C. The weak force only sees left-handed particles, which we distinguish with the subscript L. And the electroweak interaction that a particle undergoes is determined by its hypercharge Y. For example, the quarks all have a non-zero color and non-zero hypercharge, so they participate in the strong and electromagnetic interactions. If a quark is left-handed, it will also feel the weak interaction. The neutrinos, on the other hand, have neither charge nor color, so they are invisible to both the strong and electromagnetic force. We express this by letting their fields transform as singlets under those symmetry groups.

1.1 Beyond the Standard Model

Together, these three interactions make up the Standard Model gauge group $\mathrm{SU}(3)_C \times \mathrm{SU}(2)_L \times \mathrm{U}(1)_Y$. This determines the form of the three coupling constants, which numerical values must be experimentally measured. Since the vector bosons are represented by the generators, they are uniquely determined by the symmetry group. However, the scalar boson(s) and fermions are free as long as they belong to representations of the symmetry group. By this construction, modifications to fermions rather than bosons are generally easier to make, allowing us to propose amendments to the model. We will use this leniency to will examine the possibility of adding a new completely new interaction, which manifests itself as modifications to the neutrino-matter interactions.

2 Atmospheric Neutrino Flux

Atmospheric neutrinos originate from cosmic rays composed of high-energy protons interacting with nuclei in the atmosphere. These interactions ultimately produces pions, which decay as

$$\begin{aligned} \pi^+ &\to \mu^+ + \nu_\mu\,, \quad \pi^- \to \mu^- + \bar{\nu}_\mu \\ \pi^+ &\to e^+ + \nu_e\,, \quad \pi^- \to e^- + \bar{\nu}_e\,. \end{aligned} \tag{1}$$

The heavy muon ($m_\mu \approx 200 m_e$) decays further:

$$\mu^+ \to e^+ + \nu_e + \bar{\nu}_\mu\,, \quad \mu^- \to e^- + \bar{\nu}_e + \nu_\mu\,, \tag{2}$$

producing even more neutrinos.

The flux is provided in [1, 2], and a selection is shown in Table 1. The flux data is binned in $\cos(\theta_z)$. The fluxes are averaged over the azimuthal direction and solar minimum/maximum. The units of the fluxes are given as $\mathrm{GeV}^{-1}\,\mathrm{m}^{-2}\,\mathrm{s}^{-1}\,\mathrm{sr}^{-1}$ and are omitted from the table for clarity. We note that the fluxes for ν_τ and $\bar{\nu}_\tau$ are missing. Kaons do not decay into ν_τ. Thus, we never have to use probabilities in the form $P_{\tau\beta}$, since we have no starting atmospheric ν_τ flux. Interpolating the data yields makes us capable of approximating all four necessary fluxes for a given true energy and true zenith. The result of ϕ_μ is shown in Fig. 1. We see that the flux is almost entirely zenith independent. The energy dependence of the flux is approximately $E^{-2.7}$, so our expected event count at higher energies will suffer from this substantial decline in flux.

E [GeV]	ϕ_μ	$\phi_{\bar{\mu}}$	ϕ_e	$\phi_{\bar{e}}$	$\cos(\theta_z)$
27825	6.06×10^{-12}	3.17×10^{-12}	1.56×10^{-13}	1.04×10^{-13}	[-0.2, -0.1]
247707	5.94×10^{-16}	2.92×10^{-16}	1.36×10^{-17}	8.12×10^{-18}	[-0.7, -0.6]
22	3.33×10^{-2}	2.78×10^{-2}	9.57×10^{-3}	7.15×10^{-3}	[-0.3, -0.2]
432876	5.19×10^{-17}	2.32×10^{-17}	1.46×10^{-18}	9.83×10^{-19}	[-1.1, -1.0]
64280	1.58×10^{-13}	8.10×10^{-14}	3.49×10^{-15}	2.21×10^{-15}	[-0.4, -0.3]

Table 1: A selection of processed atmospheric South Pole fluxes from [1] by Honda et al. [2].

We propagate the atmospheric neutrino flux $\phi_\alpha^{\mathrm{atm}}(E, \theta_z)$ through the Earth. The oscillation probability $P_{\alpha\beta}$ acts as a weight to the atmospheric flux, yielding the propagated flux for flavor β at detector level as

$$\phi_\beta^{\mathrm{det}} = \sum_\alpha P_{\alpha\beta} \phi_\alpha^{\mathrm{atm}}\,, \tag{3}$$

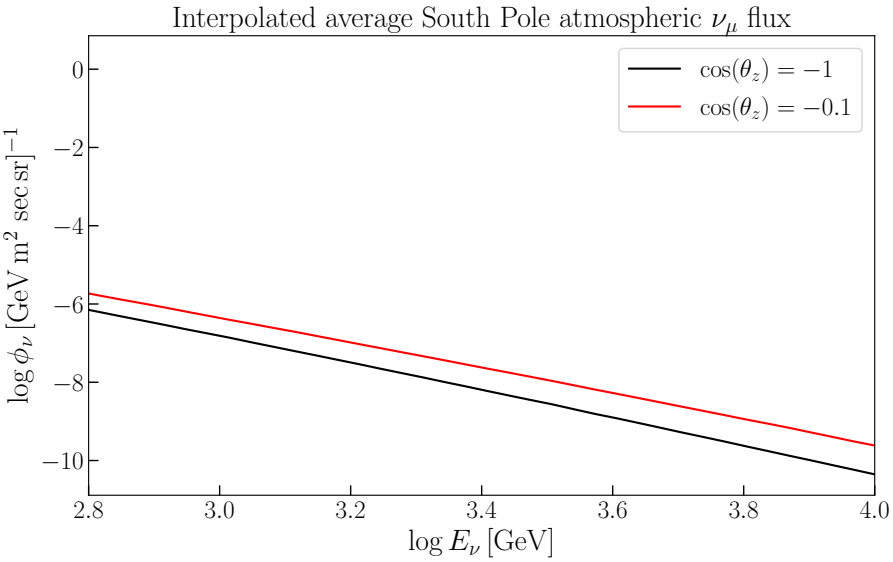

Figure 1: Interpolated South Pole atmospheric ν_μ flux with data from [2], displaying a weak zenith angle dependence, but a strong energy dependence. The energy dependence can be parametrized to be approximated by $E^{-2.7}$.

where we sum over the initial lepton flavors $\alpha \in \{e, \mu, \bar{e}, \bar{\mu}\}$.

3 Neutrino Detection

We always observe neutrinos indirectly. Regardless of the type of interaction (charged current via the W boson, or neutral current via the Z), a quark or charged lepton exits with altered properties. In the case of CC interactions, the fermion gets its flavor and energy changed, as seen in Eq. 4 where an incoming neutrino of flavor α scatters of a fermion or hadron N, producing a charged lepton α, and N' with charge changed by one unit.

$$\nu_\alpha + N \to \alpha + N' \tag{4}$$

This fermion is directly involved in the interaction with the neutrino, either as both incoming and outgoing particles, or as only the outgoing particle in the case of a hadronic interaction.

In NC interactions, shown in Eq. 5, no flavor change can occur, so the fermion leaves with increased energy. The flavor and charge of the fermion or hadron N interacting with the neutrino are unchanged. However, energy from the neutrino will be transferred to the fermion that violently recoils, later producing a shower of

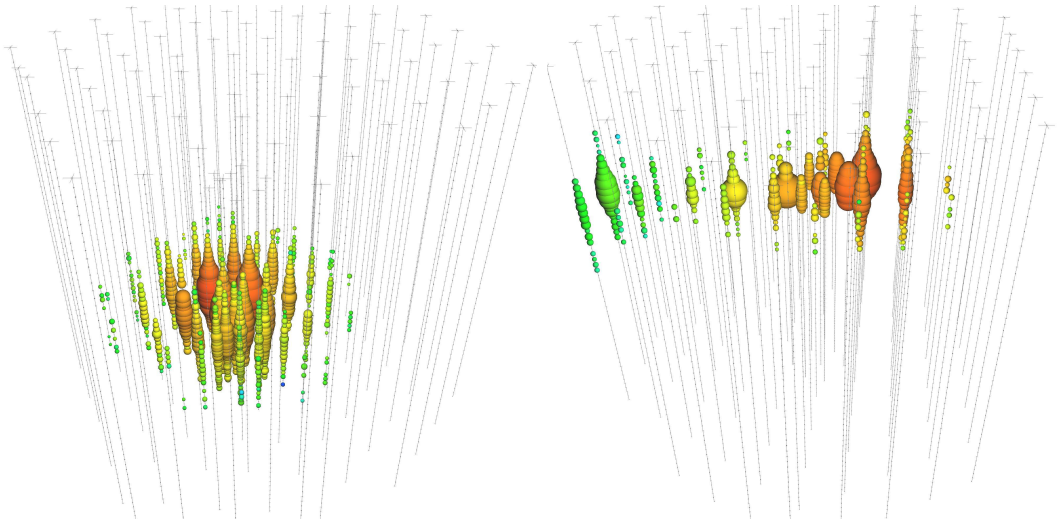

(a) Event classified as cascade, caused by an interaction in Eq. 6.

(b) Event classified as track, caused by the interaction in Eq. 7.

Figure 2: The two event types distinguished in the IceCube detector.

tertiary particles.

$$\nu_\alpha + N \to \nu_\alpha + N' \tag{5}$$

In this work, we only study the detectors buried within the Antarctic ice by the IceCube collaboration. They are of Cherenkov type, which means that they detect a fermion by its emitted Cherenkov light, produced from its travel through the ice. If the secondary particles interact heavily with the ice, they will only travel a short distance. They then decay into a shower which emits a localized flash of Cherenkov light. This event is referred to as a cascade. NC interactions tend to be classified as cascades due to the production of a localized hadronic shower However, CC ν_e interactions can also produce a similar localized flash of Cherenkov light, causing them to also contribute to the cascade events. So what about CC ν_τ? Due to the heaviness of the τ, it rapidly decays - primarily into hadrons - giving us a short path of travel with a final shower, thus manifesting themselves as a cascade [3]. A cascade event is shown in Fig. 2a and Eq. 6, shows the possible interactions causing a cascade event. Here N denotes an incoming nucleon (consisting of one fermion due to interact with the neutrino), and the resultant N' can be a hadron or a hadronic shower.

$$\begin{aligned} \nu_\alpha + N &\to \nu_\alpha + N' \\ \nu_e + N &\to e + N' \\ \nu_\tau + N &\to \tau + N' \,. \end{aligned} \tag{6}$$

If the charged leptons do not interact as much in the ice, they penetrate a larger part of it, emitting light and tertiary particles as they go. This event is called a track and is often due to charged current muon interactions. A track event is shown in Fig. 2b, and and Eq. 7 shows the possible interactions causing a track event.

$$\nu_\mu + N \to \mu + N' \tag{7}$$

So NC interactions and CC ν_e, ν_τ interactions produce cascades, while CC ν_μ interactions produce tracks. The charged secondary N' is then detected (or, in the case of CC ν_τ, a tertiary shower from the τ decay), and the properties of the neutrino involved in the interaction are then deduced. This deduction will be imperfect, and this introduces complexities that we will handle in Ch. 4. However, the detection of the topologies themselves is also not straightforward, and misclassifications are bound to occur. We see this from classifications from 'Sample B' of a 2019 DeepCore study [3], from which we summarize the classification information in Table 2.

Interaction	Track	Cascade
CC ν_e	30%	70%
CC ν_μ	70%	30%
CC ν_τ	29%	71%
NC ν	24%	76%

Table 2: The neutrino event classification at 56 GeV from 'Sample B' in [3], showing how simulated events where classified.

In order to detect the Cherenkov light, 60 Digital Optical Modules (DOMs) are placed on a long string up to 17 m apart. 86 of these strings are then lowered into 2.5 km deep boreholes in the ice. The holes are then sealed by refreezing the ice, resulting in a total of 5160 DOMs in a volume of approximately 1 km^3 [4].

The strings and DOMs are not spaced evenly, making some parts of the detector more sensitive to certain energy ranges than others. 8 strings packed more tightly than the other 78, making that part of the detector sensitive to neutrino energies down to single-digit GeV. This detector is referred to DeepCore. DeepCore will be treated as a separate and independent detector from the rest of the array, which retains the name IceCube. A view of the current setup can be seen in Fig. 3. In this work, we consider DeepCore data between 5.6 GeV to 56 GeV and IceCube data in the range 0.5 TeV to 10 TeV.

In 2017, the PINGU Letter of Intent was published [5]. The 'Precision IceCube Next Generation Upgrade' is an upgrade that will supplement DeepCore, i.e. boosting the capabilities of neutrino detection at the GeV scale. As the PINGU upgrade is not yet financed nor built, we are unable to use any data from it. However, the collaboration has released preliminary simulations, which we will use. The

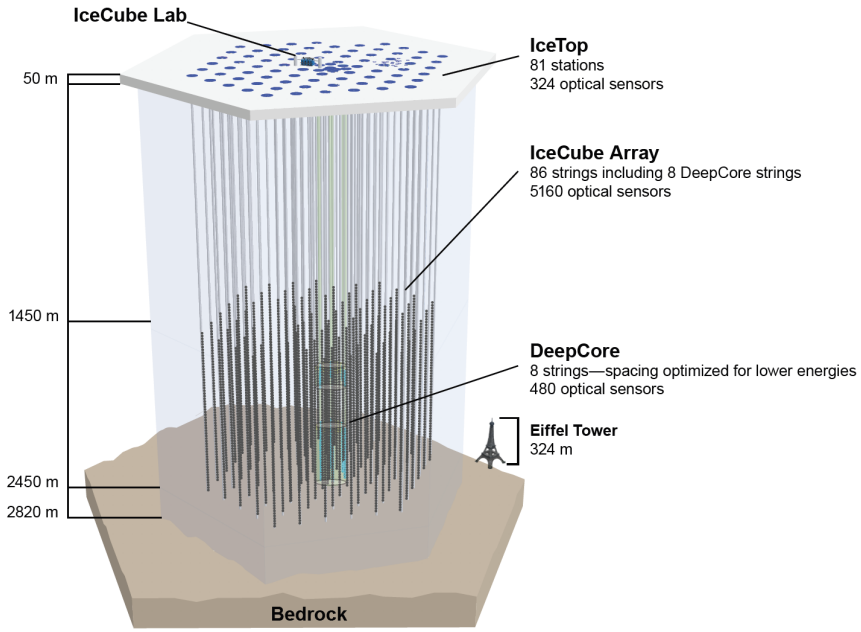

Figure 3: View of the full IceCube array, with the Eiffel tower for scale.

simulated events are between 5.6 GeV to 56 GeV, the same range as the DeepCore data. The PINGU simulations have the same structure as the DeepCore data, so our analysis referring to DeepCore will also apply to PINGU except where noted. However, we treat the PINGU detector as independent of the other experiments.

3.1 True and Reconstructed Parameters

After an event has occurred, the IceCube collaboration *reconstruct* the event. Given the parameters recorded by the detector, what are their 'true' values? We are interested in two variables: energy and direction. Each event is tagged with a probable energy and zenith angle, called the reconstructed parameters E^{reco} and $\cos(\theta_z^{reco})$, which are the parameters according to the DOMs. In other words, the collaboration uses the recorded data to backtrack the event, using the reconstructed parameters to approximate the true parameters. So a charged lepton hits the DOMs, and we ultimately end up with the associated neutrino's true energy and zenith angle, E^{true} and $\cos(\theta_z^{true})$. The reconstructed parameters are what we are using to analyze the data (because this is what the detector sees), while the true parameters are used in the determination of that neutrino's 'actual' flux and cross-section (because this is what Nature sees).

How do we then translate between the reconstructed and true parameters? In this work, we are using two different methods, which are based on the form of data

available to us. They will be outlined in Sec. 4 and Sec. 5.

4 IceCube

As the neutrinos have propagated the Earth, they arrive at the South Pole, where they interact with charged leptons in the ice. The charged lepton then emits the Cherenkov light detected by the array. We construct the event rate for each bin as

$$N_{ij} = T \sum_{\beta} \int_{(\cos\theta_z^r)_i}^{(\cos\theta_z^r)_{i+1}} \mathrm{d}\cos\theta_z^r \int_{E_j^r}^{E_{j+1}^r} \mathrm{d}E^r \int_0^{\pi} R(\theta^r, \theta^t) \mathrm{d}\cos\theta^t \int_0^{\infty} R(E^r, E^t) \phi_\beta^{\mathrm{det}} A_\beta^{\mathrm{eff}} \mathrm{d}E^t \,, \tag{8}$$

where T is the live time of the detector, β the final neutrino flavors, θ_z^r the reconstructed zenith angle, i.e. the deduced direction of the incoming neutrino binned with index i. θ_z^t is the true zenith angle, i.e. the actual direction of the incoming neutrino. E^r is the reconstructed energy, binned with index j. $R(\theta^r, \theta^t)$ is a zenith resolution function that describes the relationship with the reconstructed and true zenith angles, specific to the 86-string configuration of IceCube. $R(E^r, E^t)$ is an energy resolution function that describes the relationship with the reconstructed and true energies. $\phi_\beta^{\mathrm{det}}$ is the conventional atmospheric neutrino flux for flavor β, propagated to detector level in accordance with Eq. 3.

We now are interested in the effective area A^{eff}, i.e. the cross-sectional area of the detector that the lepton is exposed to. A^{eff} depends on several parameters, some of them being physical detector volume, E^{true}, $\cos(\theta_z^{true})$, and the particle type. Fortunately, the binned A^{eff} is provided to us by the collaboration [6]. An excerpt from this data is shown in Table 3.

E_{min}^{true} [GeV]	E_{max}^{true} [GeV]	$\cos(\theta_z^{true})_{min}$	$\cos(\theta_z^{true})_{max}$	A^{eff} [m^2]
251	316	-0.92	-0.91	0.0174
794300	1000000	-0.80	-0.79	69.3600
3981	5012	-0.78	-0.77	3.1490
1585	1995	-0.07	-0.06	0.4659
398	501	-0.73	-0.72	0.0555

Table 3: IceCube-86 effective area from [6].

Here, A^{eff} has been averaged over A_μ^{eff} and $A_{\bar{\mu}}^{\mathrm{eff}}$ by the collaboration. Thus, both μ and $\bar{\mu}$ will, on average, experience the same A^{eff} in our model. Just as with the fluxes, we interpolate this in E^{true} and $\cos(\theta_z^{true})$, and show the result in Fig. 4 Since the IceCube array is slightly rectangular, the zenith angle affects the cross-sectional area to which the array the leptons are exposed to. While the flux was almost flat in $\cos(\theta_z^{true})$, the introduction of the zenith dependent A^{eff} will make the result slightly more zenith dependent than the flux itself. Increasing linearly with energy, the effective area of the detector approaches its geometrical area of $1 \times 10^6\,\mathrm{m}^2$ but is still only in the single-digit range at TeV energies.

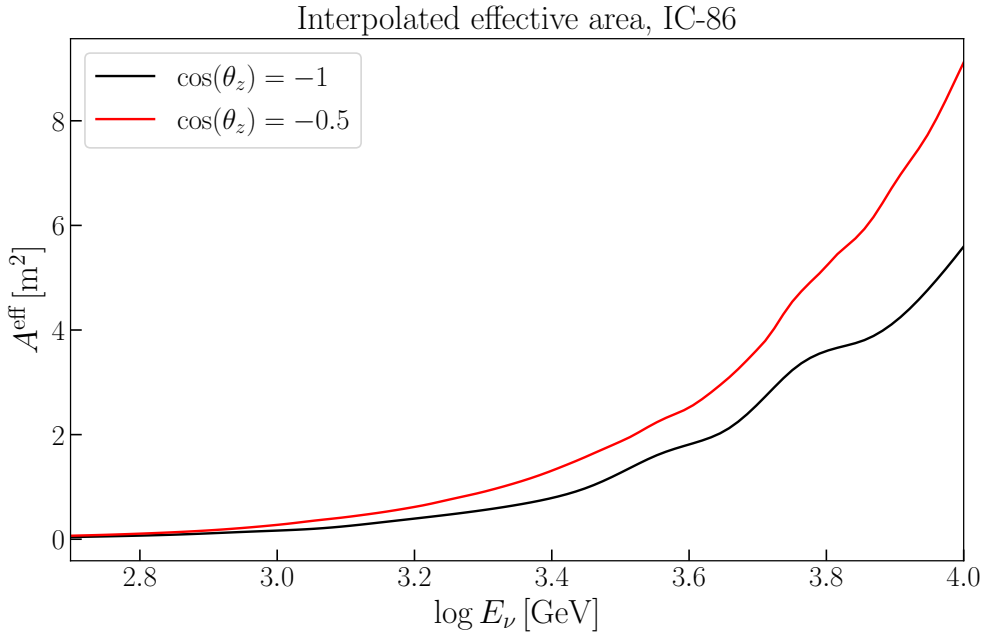

Figure 4: Interpolated IceCube effective area with data from [6].

So now we have the physical quantities in the true parameters. As we discussed, we need a way to translate this into the reconstructed parameters that the detector gives us. We will call the relationship between E^{reco} and E^{true} the energy resolution function, and the relationship between $\cos(\theta_z^{reco})$ and $\cos(\theta_z^{true})$ the zenith resolution function. We assume the relationship to follow a logarithmic Gaussian distribution, giving it the form

$$R(x^r, x^t) = \frac{1}{\sqrt{2\pi}\sigma_{x^r} x^r} \exp\left[-\frac{(\log x^r - \mu(x^t))^2}{2\sigma_{x^r}^2}\right] . \tag{9}$$

The parameters of the Gaussian are $\sigma_{x^r}(x^t)$ and $\mu(x^t)$, which are functions of the true parameters. By multiplying the Gaussian in Eq. 9, we are reweighing the values by the probability density of that point. This process is also called *smearing* because it effectively spreads out the data around a certain point.

So how do we then obtain $\sigma_{x^r}(x^t)$ and $\mu(x^t)$ needed to construct the Gaussian? A Monte Carlo sample publicly released by the collaboration has all the ingredients that we need [7]. In Table. 4 we show a selection of the data. The 'pdg' column refers to the Monte Carlo particle classification, where 13 is the tag for ν_μ, while -13 refers to an $\bar{\nu}_\mu$. Here we note a crucial property of the IceCube dataset that will impact our analysis: the MC released by the collaboration only includes simulated muon events.

First, we let $\cos(\theta_z^{reco}) = \cos(\theta_z^{true})$ for all values. The angular resolution in IceCube for track-like events is less than 2°, making $\cos(\theta_z^{true})$ coincide with $\cos(\theta_z^{reco})$

pdg	E^{reco} [GeV]	$\cos(\theta_z^{reco})$	E^{true} [GeV]	$\cos(\theta_z^{true})$
13	1665	-0.645884	592	-0.653421
13	587	-0.373241	342	-0.424979
-13	1431	-0.177786	1169	-0.189949
-13	831	-0.807226	1071	-0.805559
13	988	-0.370746	1861	-0.367922

Table 4: A selection of the data found in [7]

for our study [8]. Thus, we only need to concern ourselves with the energy resolution function. In Fig. 5, we have plotted all event counts found in the MC file, over 8 million. However, this is too much data to process efficiently, with many outliers that ultimately do not weigh in that much in the final event count. To resolve this, we have opted to train a Gaussian process regressor on the dataset, from which we can extract the predicted mean and standard deviation for a point. When doing this over E^{reco}, we sample E^{true} in the 99th percentile around the predicted mean. We then obtain the shaded band shown in Fig. 5.

Note that since atmospheric neutrino flux scales as $E^{-2.7}$, the log-normal Gaussian $R(E^r, E^t)$ as E^{-2}, and the effective area is approximately linear in E. Thus, the event count in 8 will be proportional to $E^{-1.7}$. Having almost a quadratic drop-off, the event count as observed by IceCube will be lower and lower as we probe higher energies, severely limiting our confidence in TeV analyses due to lower statistical significance.

Now, Eq. 8 handles the Gaussian smearing, but we are not provided systematic error sources, DOM efficiencies, and other nuisance parameters. To correct this, we will aim to come as close as possible to the IceCube Monte Carlo, and then normalize with it. That way, we know that our null hypotheses will align while we are free to form additional hypotheses with different physics parameters.

The latest available data collected and processed by the collaboration contains 305,735 muon track events, collected over eight years [8]. The data has 13 logarithmically spaced bins in $E^{reco} \in [500, 9976]$ GeV, and 20 linear bins in $\cos(\theta_z^{reco}) \in [-1, 0]$. The data is shown in Fig. 6.

Monte Carlo normalization

Independent researchers outside of the IceCube collaboration will not be able to simulate the detector more precisely. The IceCube Monte Carlo is a complex and proprietary machinery, so our goal in this section is merely to come as close as we can to it. After we are confident that our code displays the same overall features

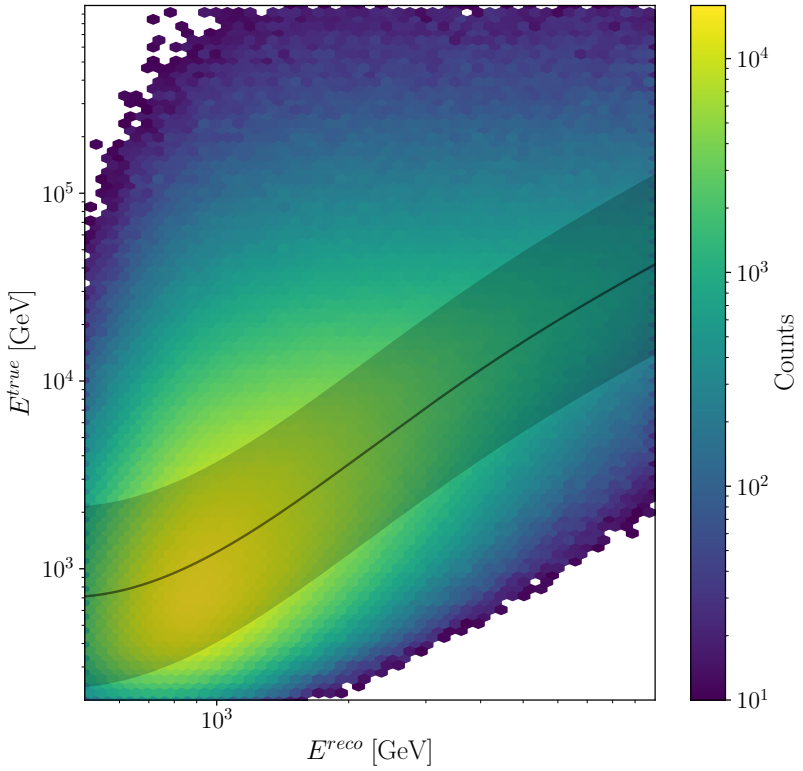

Figure 5: Relationship between the true and reconstructed muon energy in the IceCube MC sample [7]. The color indicates the frequency of each simulated point. Shaded area shows the 99th percentile limits predicted by the regressor trained on this set. It is within this band that then will sample the E^{true} values for each E^{reco}.

as the 'official', we normalize our results N_{ij}^{sim} as

$$N_{ij} = \frac{N_{ij}^{\text{null}}}{N_{ij}^{\text{MC}}} N_{ij}^{\text{sim}} \,. \tag{10}$$

For each bin i, j, we then obtain a correction factor that contains information that we are unable to obtain or sufficiently incorporate. One example of such information is the systematic errors of the DOMs. Recent IceCube data releases do not include such information. Since the systematic errors are affecting the event count on a bin-by-bin basis, they can, in theory, drastically modify the binned results. Another example of an error source that will be remedied by this method is the flux. We are using a fairly simple model of the atmospheric flux that excludes atmospheric prompt and astrophysical fluxes. The IceCube collaboration uses several different flux models, which are initialized by a parametrization of the cosmic ray flux.[1]

[1]Included in the cosmic ray models are e.g. the pion to kaon ratio, which are often used as a nuisance parameter. By not being able to include this in our error analysis, our method will be limited to only consider the overall flux normalization rather than the components that produce

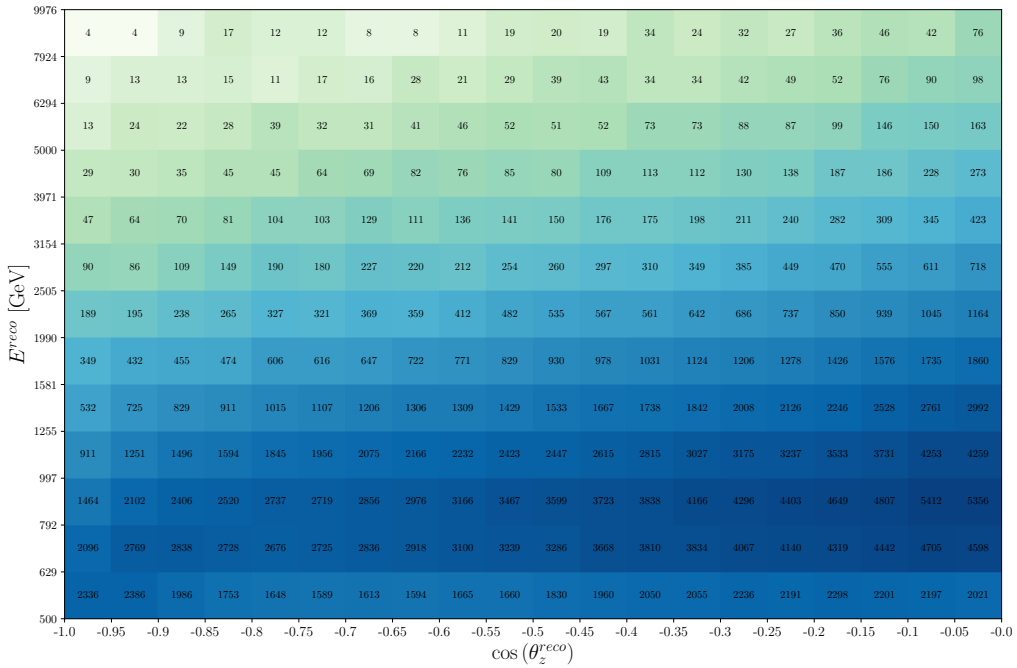

Figure 6: IceCube track events from [8], displaying the $E^{-1.7}$ drop-off in event count.

In Fig. 7, we present the IceCube Monte Carlo obtained from their 2020 sterile analysis [8], along with our null hypothesis times a constant factor. We used the best-fit values from NuFit [9] with the exception of the CP-violating phase δ_{CP}, which was set to 0° for simplicity. The values used are

$$\theta_{12} = 33.44°, \quad \theta_{13} = 8.57°, \quad \theta_{23} = 49.2°, \quad \delta_{\text{CP}} = 0° \,. \tag{11}$$

We deemed these shapes to be satisfactory, thus allowing us to multiply Eq. 8 by the correction factors of Eq. 10. Thus, we are now able to sufficiently approximate the IceCube Monte Carlo, which makes us able to run simulations based on different physics scenarios.

the flux in the first place.

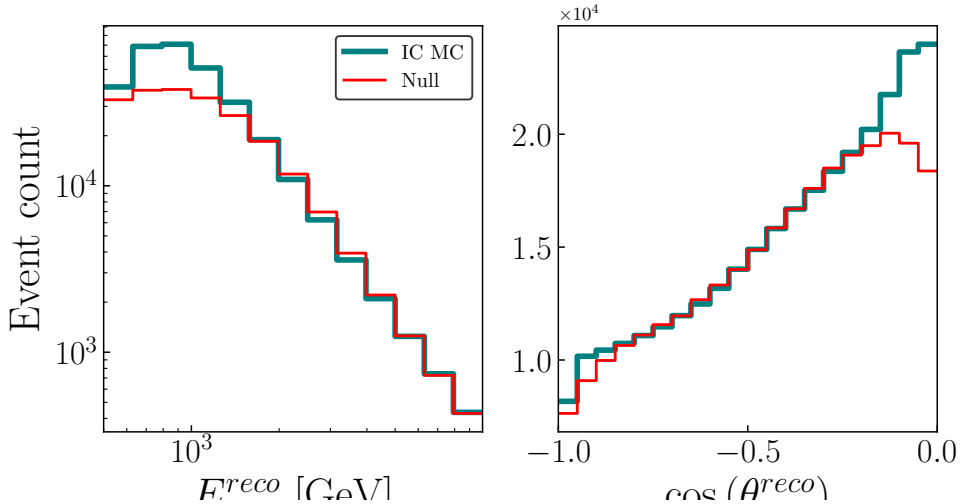

Figure 7: IceCube Monte Carlo, binned in E^{reco} and $\cos(\theta_z^{reco})$. We compare this with our simulations shown as 'Null' in red in the plots.

5 DeepCore

In this part, we use the publicly available DeepCore data sample [10] which is an updated version of what was used by the IceCube collaboration in a ν_μ disappearance analysis [11].

The detector systematics include ice absorption and scattering and overall, lateral, and head-on optical efficiencies of the DOMs. They are applied as correction factors using the best-fit points from the 2019 DeepCore ν_τ appearance analysis [3].

The data include 14901 track-like events and 26001 cascade-like events, both divided into eight $\log_{10} E^{reco} \in [0.75, 1.75]$ bins, and eight $\cos(\theta_z^{reco}) \in [-1, 1]$ bins. Each event has a Monte Carlo weight $w_{ijk,\beta}$, from which we can construct the event count as

$$N_{ijk} = C_{ijk} \sum_\beta w_{ijk,\beta} \phi_\beta^{\text{det}} \,, \tag{12}$$

where $C_{k\beta}$ is the correction factor from the detector systematic uncertainty and ϕ_β^{det} is defined as Eq. 3. We have now substituted the effect of the Gaussian smearing by treating the reconstructed and true quantities as a migration matrix.

6 PINGU

The methodology behind the PINGU simulations is the same as with our DeepCore study . We use the public MC [12], which allows us to construct the event count as in Eq. 12. However, since no detector systematics is yet modeled for PINGU, the correction factors C_{ijk} are all unity. As with the DeepCore data, the PINGU Monte Carlo is divided into eight $\log_{10} E^{reco} \in [0.75, 1.75]$ bins, and eight $\cos(\theta_z^{reco}) \in [-1, 1]$ bins for both track- and cascade-like events. We generate 'data' by predicting the event rates at PINGU with the following best-fit parameters from [9], except for the CP-violating phase, which is set to zero for simplicity.

$$\begin{aligned} &\Delta m^2_{21} = 7.42 \times 10^{-5}\,\text{eV}^2, \;\; \Delta m^2_{31} = 2.517 \times 10^{-3}\,\text{eV}^2, \\ &\theta_{12} = 33.44^\circ, \quad \theta_{13} = 8.57^\circ, \quad \theta_{23} = 49.2^\circ, \quad \delta_{\text{CP}} = 0^\circ \,. \end{aligned} \tag{13}$$

7 Non-Standard Interactions

We have no reason to believe that the Standard Model gauge group is the complete picture. We have already seen how the failure of the Standard Model to predict neutrino masses and oscillations forces us to amend it. Just as the electroweak theory $SU(2)_L \times U(1)_Y$ is spontaneously broken to $U(1)_{EM}$, a higher order theory at a different energy scale with completely different properties might undergo a similar spontaneous symmetry break at high energies, producing at lower energies the Standard Model that we know. In fact, just as the fermion masses originate from the electroweak symmetry breaking, the neutrino masses might be generated from another broken symmetry resulting in the Standard Model gauge group. In this sense, the Standard Model might be considered an effective low energy theory, which is yields impressive results in some areas but fails in others.

Compared to other fermions, the lightness of neutrino masses[2] along with their sparse SM interactions might indicate that these particles provide the best starting point for us to probe new physics, in which exotic neutrino interactions might occur [13]. We call these interactions non-standard interactions (NSI) in order to distinguish them from the 'standard' interactions of the Standard Model.

Following the approach of the Standard Model that the group generators uniquely determine the gauge bosons, a different gauge theory will have different interactions than those we presently know. These new interactions can be parametrized as model-independent four-fermion effective operators [14, 15]. Following the discussion in [16], we see that the NSI parameters ϵ resulting from six-dimensional operators have the scale

$$\epsilon \propto \frac{m_W^2}{m_\epsilon^2} \sim \frac{10^{-2}}{m_\epsilon^2} \tag{14}$$

in TeV, so the new interactions generated at a mass scale of $m_\epsilon = 1\,\text{TeV}$ will produce parameters in the order of 10^{-2}, two magnitudes below the standard matter effect. Thus, if we assume the new interactions to arise from a higher-energy theory above electroweak scale, we then predict that the parameters contribute with at most a factor of 10^{-2} to the standard matter effect, decreasing quadratically.

7.1 Non-Standard Effects on Neutrino Matter Interactions

Up until now, we have only considered weak neutrino interactions with electrons, protons, and neutrons. We can phenomenologically allow these interactions to include the up and down quarks which are present in the Earth as the fundamental

[2]The extreme lightness might be explained by a mass generation at a higher order theory.

components of neutrons and protons, as seen in the Lagrangians

$$\mathcal{L}_{\rm CC} = -2\sqrt{2}G_F\epsilon^{ff'X}_{\alpha\beta}\left(\bar{\nu}_\alpha\gamma^\mu P_L\ell_\beta\right)\left(\bar{f}'\gamma_\mu P_X f\right)$$
$$\mathcal{L}_{\rm NC} = -2\sqrt{2}G_F\epsilon^{fX}_{\alpha\beta}\left(\bar{\nu}_\alpha\gamma^\mu P_L\nu_\beta\right)\left(\bar{f}\gamma_\mu P_X f\right)\ ,$$

where CC denotes the charged current interaction with the matter field $f \neq f' \in \{u, d\}$, and NC denotes the neutral current interaction with $f \in \{e, u, d\}$. The CC NSI effect affects neutrino production and detection, and will not be considered further. NC NSI affect the matter potential, and is thus of interest to us.

We have no independent sensitivity for the neither chirality nor flavor type of ϵ^X, so we sum over these and study the effective matter NSI parameter $\epsilon_{\alpha\beta}$:

$$\epsilon_{\alpha\beta} = \sum_{X\in\{L,R\}}\sum_{f\in\{e,u,d\}}\frac{N_f}{N_e}\epsilon^{fX}_{\alpha\beta}\ . \tag{15}$$

Our matter study will be wholly confined to the interior of the Earth, where we assume electrical neutrality and equal distribution of neutrons and protons, we get $N_u/N_e \simeq N_d/N_e \simeq 3$. Also we assume the components $\epsilon_{\alpha\beta}$ to be real. Thus,

$$\epsilon_{\alpha\beta} = \sum_X \epsilon^{eX}_{\alpha\beta} + 3(\epsilon^{uX}_{\alpha\beta} + \epsilon^{dX}_{\alpha\beta}) \tag{16}$$

Now, $\epsilon_{\alpha\beta}$ enters the Hamiltonian as entries of a potential-like matrix. In Eq. 17, $A_{CC}\text{diag}(1,0,0)$ is our familiar matter potential from the Standard Model. There is also our new term, $A_{CC}\epsilon$, which contains the components $\epsilon_{\alpha\beta}$:

$$\begin{aligned} H &= \frac{1}{2E}\left[UM^2U^\dagger + A_{CC}\,\text{diag}(1,0,0) + A_{CC}\,\epsilon\right] \\ &= \frac{1}{2E}\left[UM^2U^\dagger + A_{CC}\begin{pmatrix}1+\epsilon_{ee} & \epsilon_{e\mu} & \epsilon_{e\tau}\\ \epsilon_{\mu e} & \epsilon_{\mu\mu} & \epsilon_{\mu\tau}\\ \epsilon_{\tau e} & \epsilon_{\tau\mu} & \epsilon_{\tau\tau}\end{pmatrix}\right]\ . \end{aligned} \tag{17}$$

In the limit $\epsilon_{\alpha\beta} \to 0$, we recover the standard interaction Hamiltonian from Eq. **??**. We can draw several conclusions from this form of the Hamiltonian. Any nonzero off-diagonal element $\epsilon_{\alpha\beta}, \alpha \neq \beta$ contribute to neutrino mixing, just as the off-diagonal elements of U does in the SM. Moreover, since the SM potential has the same order in A_{CC} as the NSIs, any $\epsilon_{\alpha\beta} \sim 1$ will make the new matter effect be the same order as the SM effect.

We have two more modifications to the matrix ϵ. First, all terms of the Hamil-

tonian must of course be Hermitian, thus

$$\begin{pmatrix} \epsilon_{ee} & \epsilon_{e\mu} & \epsilon_{e\tau} \\ \epsilon_{\mu e} & \epsilon_{\mu\mu} & \epsilon_{\mu\tau} \\ \epsilon_{\tau e} & \epsilon_{\tau\mu} & \epsilon_{\tau\tau} \end{pmatrix} = \begin{pmatrix} \epsilon_{ee} & \epsilon_{e\mu} & \epsilon_{e\tau} \\ \epsilon_{e\mu} & \epsilon_{\mu\mu} & \epsilon_{\mu\tau} \\ \epsilon_{e\tau} & \epsilon_{\mu\tau} & \epsilon_{\tau\tau} \end{pmatrix} . \tag{18}$$

Now we have reduced the possible number of NSI parameters from 9 down to 6.

By combining oscillation data and neutrino-nucleon scattering at the COHERENT experiment, 90 % CL ranges of some of the NSI parameters were constrained in [17] to

$$\begin{aligned} -0.090 < \epsilon_{\tau\tau} < 0.38 \\ -0.01 < \epsilon_{\mu\tau} < 0.009 \\ -0.073 < \epsilon_{e\mu} < 0.044 \\ -0.15 < \epsilon_{e\tau} < 0.13 \, . \end{aligned} \tag{19}$$

7.2 IceCube Signal

The effect of NSI on the IceCube event count has been previously discussed in [14, 18, 15]. In our analysis of IceCube, we are constrained to muon track events. Thus, we are not able to test any theory which does not modify $P_{\alpha\mu}$. Moreover, the IceCube data is available in the range 500 GeV to 10 TeV range, where any rapid oscillations have averaged out.

Since all standard matter potentials are diagonal, the elements $\epsilon_{\alpha\beta}$, $\alpha = \beta$ will directly adjust the matter potential felt by flavor α. The off-diagonal terms have a more interesting theoretical implication as they open up matter interactions across flavors. Remember, in the Standard model, we are restricted to weak interactions that conserve lepton flavor. However, an off-diagonal NSI parameter allows flavor transitions during matter interactions. Thus, the off-diagonal elements constitute new sources of flavor violation. Moreover, $\epsilon_{\alpha\beta}$ modifies the $\nu_\alpha \to \nu_\beta$ transition independently of the mixing matrix. Thus, we are not confined to the parameters of the mixing matrix: now we have introduced the possibility of additional interactions that can cause the flavor change. Moreover, since we have six NSI parameters, and the PMNS matrix is parametrized with only three parameters, we have more degrees of freedom when adjusting the probabilities using the NSI matrix. Each term in the PMNS matrix consists of at least two of the three mixing angles. This makes the individual angles more inter-dependent than the NSI parameters since combinations of them must satisfy the constraints of the matrix elements.

As discussed in Eq. **??**, the atmospheric $\nu_\mu \to \nu_\tau$ transition will be the most abundant, making $\epsilon_{\mu\tau}$, $\epsilon_{\mu\mu}$, $\epsilon_{\tau\tau}$ the most suitable NSI parameters to constrain from muon events. As we will see, $\epsilon_{e\mu}$ is also a candidate, albeit a weaker one.

In Fig. 8, we see how the introduction of $\epsilon_{\mu\tau} = 0.02$ alters the ν_μ and $\bar{\nu}_\mu$ survival probabilities for neutrinos that traverse the entire Earth diameter (i.e. $\cos(\theta_z^{true}) = -1$). $\epsilon_{\mu\tau}$ does not dramatically change neither amplitude nor frequency of the probabilities. Instead, it seems to stretch or compress the oscillations. Since the only difference between the way neutrinos and antineutrinos interact with matter is the sign of the potential, the probability for ν_μ with positive $\epsilon_{\alpha\beta}$ is identical to the probability for $\bar{\nu}_\mu$ with negative $\epsilon_{\alpha\beta}$. Thus, the dashed line in the right panel not only shows the survival probability for $\bar{\nu}_\mu$ with $\epsilon_{\mu\tau} = 0.02$, but also the survival probability for ν_μ with $\epsilon_{\mu\tau} = -0.02$. Hence, we note that $\epsilon_{\mu\tau} > 0$ stretches (compresses) $P_{\mu\mu}$ for neutrinos (antineutrinos), while $\epsilon_{\mu\tau} < 0$ compresses (stretches) $P_{\mu\mu}$ for neutrinos (antineutrinos).

The value of $\epsilon_{\tau\tau}$ affects neither $P_{\mu\mu}$ nor $P_{\bar{\mu}\bar{\mu}}$, in the IceCube region above 500 GeV. Hence, we will not be able to say anything about $\epsilon_{\tau\tau}$ in our IceCube study. Comparing the probabilities in Fig. 8 with $\epsilon_{\tau\tau} = 0.05$ with the ones for $\epsilon_{\mu\tau} = 0.02$ in Fig. 8, we see that even though we let $\epsilon_{\tau\tau}$ take 2.5 times the value of $\epsilon_{\mu\tau}$, its effect on $P_{\mu\mu}$ is smaller. The weakening of the $P_{\bar{\mu}\bar{\mu}}$ resonance will be visible in DeepCore, but we should expect a less stringent constraint due to the weakness of the effect compared to $\epsilon_{\mu\tau}$.

Thus, we will use IceCube to constrain $\epsilon_{\mu\tau}$ only.

Moving on to $\epsilon_{e\mu}$ and Fig. 9, we see that both probabilities has shifted downwards for $E^{true} > 500$ GeV. In Fig. 9, we see that the muon channel remains largely unaffected of the value of $\epsilon_{e\tau}$ as we expected. The exception of this lies in the DeepCore region of rapid oscillations, where mixing is more violent.

7.3 DeepCore and PINGU Signals

The effect of NSI on the DeepCore event count has been previously discussed in [19], while the NSI effect in PINGU has been studied in [20, 21]. Now we repeat our probability analysis but for the DeepCore/PINGU region of 5.6 GeV to 56 GeV. As we previously saw, we have rapid oscillations, which means that 'indirect' modifications (i.e. $\epsilon_{e\tau}$ will affect the $P_{\mu\mu}$ channel) will be more apparent since all flavors are involved to a greater degree compared with the more stable region above 500 GeV, where many oscillations have averaged out.

Another feature of our DeepCore study includes the fact that we now have access to cascade events, in which ν_e and ν_τ are more abundant. Thus, we are no longer constrained to the μ channel alone, but we can now find interesting features in the other channels too. However, we remember that the ν_μ flux is still the most abundant.

Fig. 10 shows the electron neutrino and antineutrino survival probabilities, and here we see a clear signal when turning on $\epsilon_{e\tau}$.

Fig. 8 shows that $\epsilon_{\mu\tau}$ affects both $P_{\mu\mu}$ and $P_{\bar{\mu}\bar{\mu}}$ over the whole energy range.

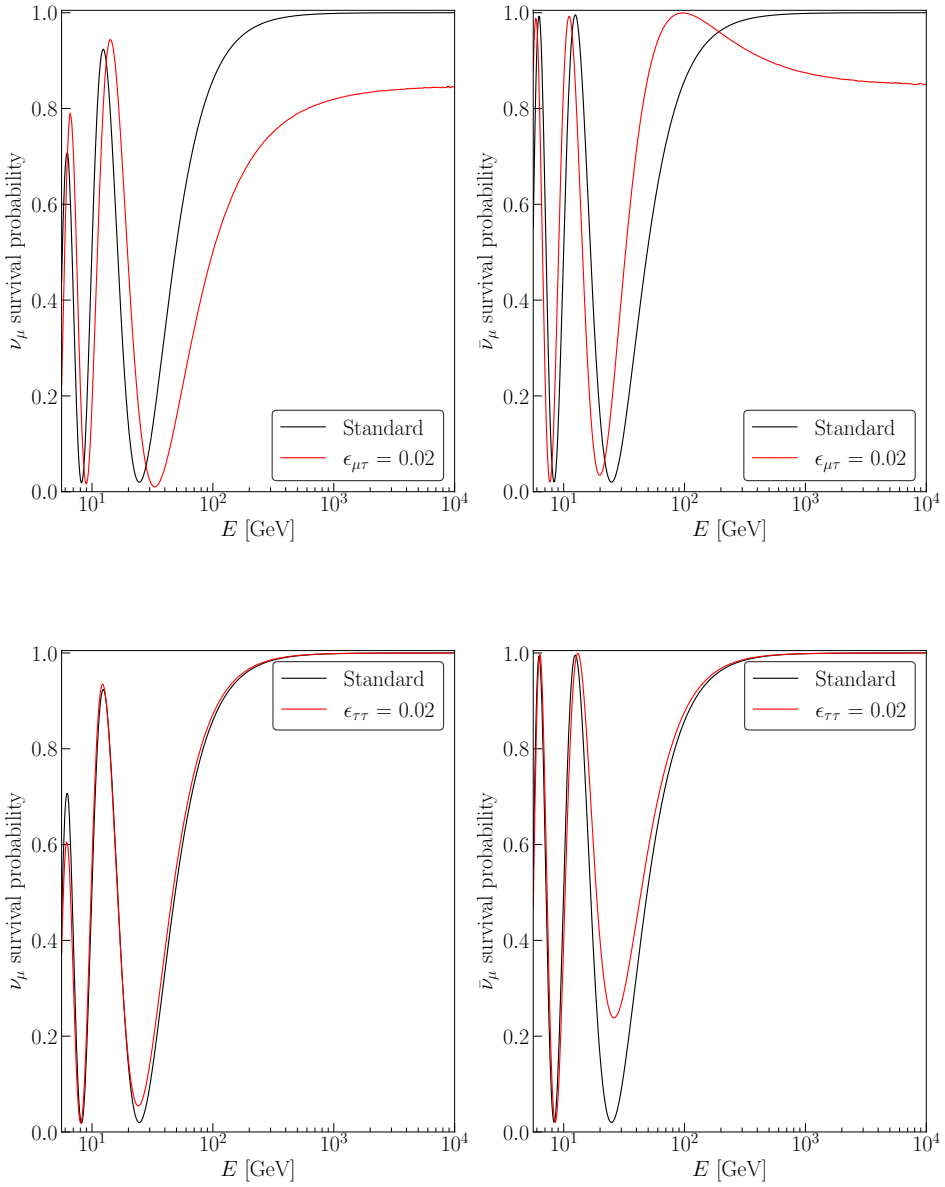

Figure 8: *Top panel:* Muon neutrino and antineutrino survival probabilities for $\cos(\theta_z^{true}) = -1$ when $\epsilon_{\mu\tau} = 0.02$. All other NSI parameters are fixed to zero. In the GeV range, $\epsilon_{\mu\tau}$ shifts the oscillations to the right for ν_μ, and to the left for $\bar{\nu}_\mu$. At TeV energies, both probabilities simply get shifted down, resulting in a net reduction of track events. *Bottom panel:* Muon neutrino and antineutrino survival probabilities for $\cos(\theta_z^{true}) = -1$ when $\epsilon_{\tau\tau} = 0.05$. All other NSI parameters are fixed to zero. $\epsilon_{\tau\tau}$ does not affect the probabilities above 100 GeV and this parameter is thus unable to be constrained by tracks in IceCube in our study. However, the dampening of the $\bar{\nu}_\mu$ survival probability will be visible to DeepCore and PINGU, since it occurs within their energy ranges.

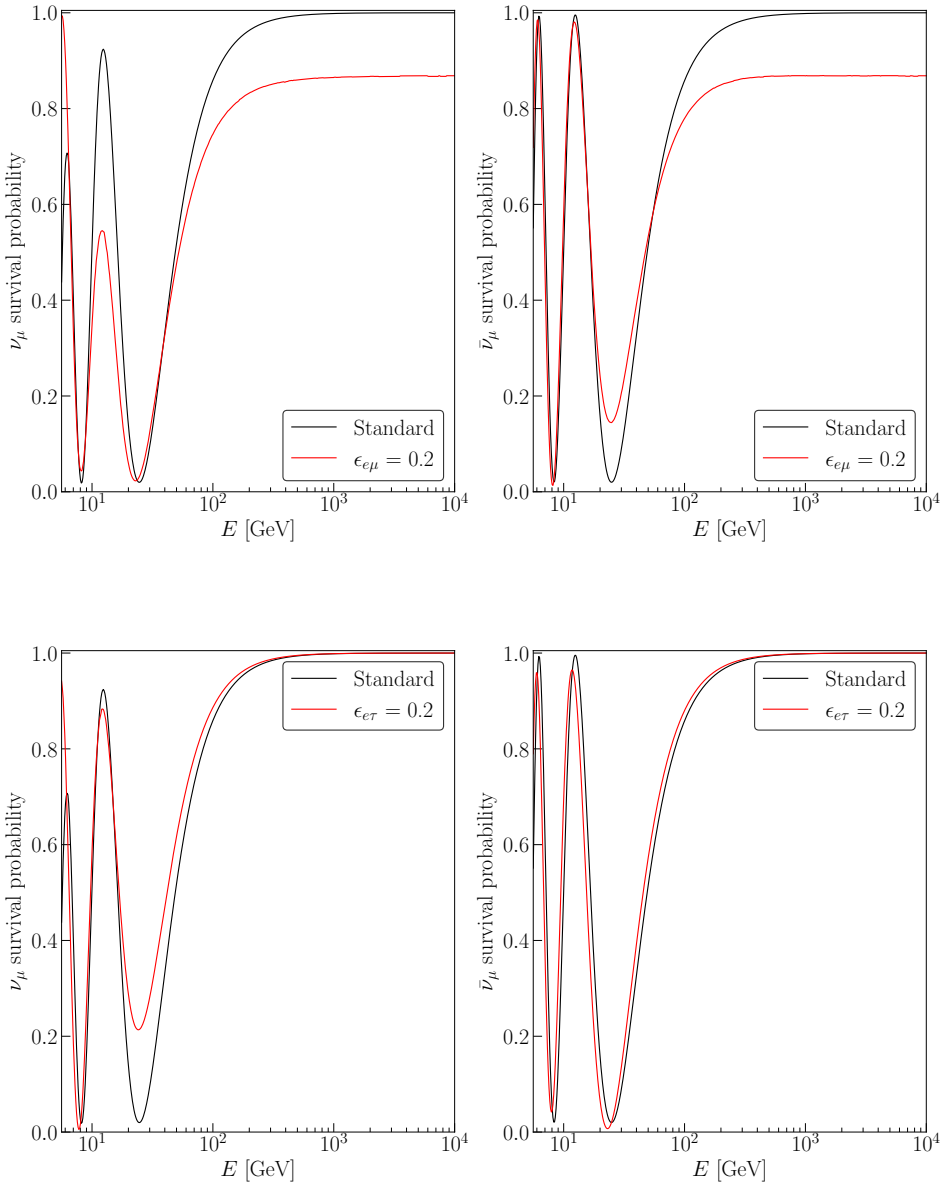

Figure 9: Muon neutrino and antineutrino survival probabilities for $\cos(\theta_z^{true}) = -1$. *Top panel:* $\epsilon_{e\mu} = 0.2$. All other NSI parameters are fixed to zero. Instead of the oscillations shifting to the left or right, $\epsilon_{e\mu}$ dampens an oscillation peak for low GeV. At TeV, the probability is shifted down, just as with $\epsilon_{\mu\tau}$. *Bottom panel:* $\epsilon_{e\tau} = 0.2$. All other NSI parameters are fixed to zero. Here, we see a very weak shifting and a ν_μ weaker dip at low GeV, and again, no visible effect at TeV energies.

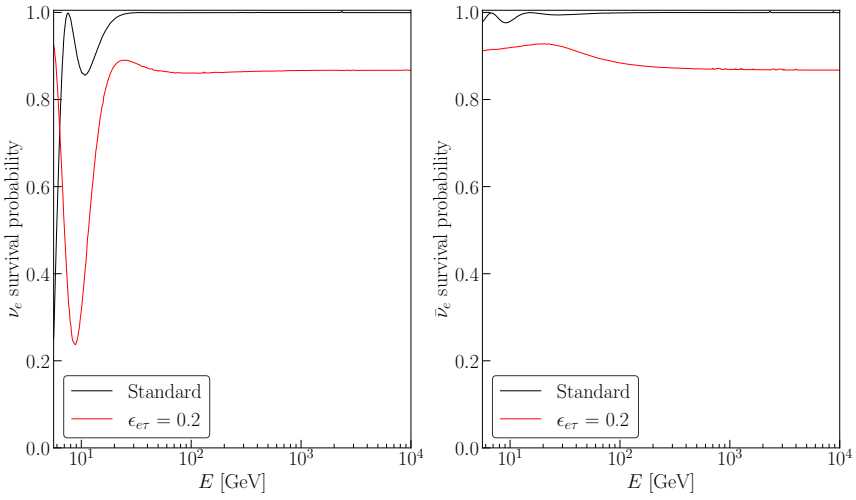

Figure 10: Electron neutrino and antineutrino survival probabilities for $\cos(\theta_z^{true}) = -1$ when $\epsilon_{e\tau} = 0.2$. All other NSI parameters are fixed to zero. Here we see a strong difference across the whole energy range, in contrast to the ν_μ and $\bar{\nu}_\mu$ plots in Fig 9.

Since IceCube also sees this, we hope to be able to boost the constraining of $\epsilon_{\mu\tau}$ by combining the two experiments.

Regarding $\epsilon_{\tau\tau}$ in Fig. 9, the signal mainly shows in the $P_{\bar{\mu}\bar{\mu}}$ channel as a shallower dip in the 20 GeV region. Thus, DeepCore/PINGU alone will be used to constrain this parameter.

$\epsilon_{e\mu}$ in Fig. 9 causes a weaker dip for both ν_μ and $\bar{\nu}_\mu$.

For $\epsilon_{e\tau}$, we see a similar effect on the dip in $P_{\mu\mu}$ as we did with $\epsilon_{\tau\tau}$ for $P_{\bar{\mu}\bar{\mu}}$. Hence, we should be able to see the $\epsilon_{e\tau}$ effect in DeepCore/PINGU. Remember that we now have the option to look at the other flavor channels than μ since we have cascade events for DeepCore and PINGU. If we simulate $P_{\mu e}^{NSI}$ at three different energies, and let both $\epsilon_{e\mu}$ and $\epsilon_{e\tau}$ vary together between the values $\{-0.3, 0.3\}$, we produce a two-dimensional grid of probabilities. Subtract the regular $P_{\mu e}^{SI}$ (that is, no NSI), and take the absolute value of the difference. We see the result in Fig. 11. The middle and right panels, which show the absolute probability difference at 25 and 50 GeV, respectively, are very bleak, indicating that the impact of the NSI parameters $\epsilon_{e\mu}$ and $\epsilon_{e\tau}$ is not as strong at these energy levels. Turning to the left-most panel, we see a region in which the difference again is close to zero, but now surrounded by fringes of very large differences, up to 50% difference in the $P_{\mu e}$ probability. This indicates that the NSI parameters are much more influential at these energies, and that we should be able to constrain both $\epsilon_{e\mu}$ and $\epsilon_{e\tau}$ from 5 GeV cascade events.

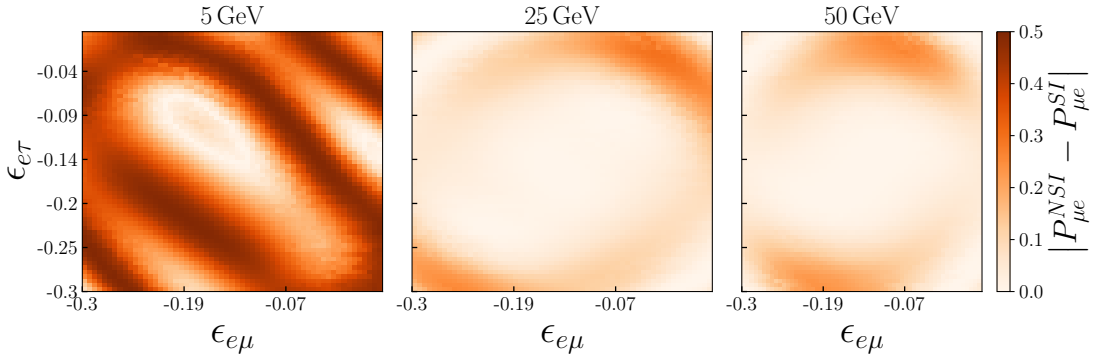

Figure 11: The quantity $\left|P_{\mu e}^{NSI} - P_{\mu e}^{SI}\right|$ when we let $\epsilon_{e\mu}$ and $\epsilon_{e\tau}$ independently vary over the range {-0.3,0.3} at 5, 25, and 50 GeV. At 5 GeV, we see strong deviations in the probabilities, showing a promising indication that constriction of $\epsilon_{e\mu}$ and $\epsilon_{e\tau}$ is possible using cascade events at these energies.

8 The NSI Hypothesis

In this section, we will constrain the four NSI parameters $\epsilon_{\tau\tau}$, $\epsilon_{\mu\tau}$, $\epsilon_{e\mu}$, and $\epsilon_{e\tau}$. As we shall see, the impacts of NSI mainly manifest themselves at GeV energies, causing us to bring back DeepCore and PINGU. We will consider the results obtained from these three detectors separately as well as jointly.

8.1 χ^2 Minimization

For our analyses, we define our χ^2 as

$$\chi^2(\hat{\theta}, \alpha, \beta, \kappa) = \sum_{ijk} \frac{\left(N^{\text{th}} - N^{\text{data}}\right)^2_{ijk}}{\left(\sigma^{\text{data}}_{ijk}\right)^2 + \left(\sigma^{\text{syst}}_{ijk}\right)^2} + \frac{(1-\alpha)^2}{\sigma^2_\alpha} + \frac{\beta^2}{\sigma^2_\beta} \tag{20}$$

where we minimize over the model parameters $\hat{\theta} \in \{\Delta m^2, \theta_{23}, \epsilon\}$, the penalty terms α and β, and the free parameter κ. N^{th}_{ijk} is the expected number of events from theory in bin $\{i, j, k\}$, where i denotes the E^{reco} bin, j denotes the $\cos(\theta_z^{reco})$ bin, and k denotes the event-type bin, i.e. track or cascade. N^{data}_{ijk} is the observed number of events in that bin. $\sigma^{\text{data}}_{ijk}$ is the experimental uncertainty, and $\sigma^{\text{syst}}_{ijk}$ the uncorrelated systematic uncertainty.

In our simulations of N^{th}_{ijk}, we set all standard oscillation parameters to their current best-fit values of Eq. 13, except for Δm^2_{31} and θ_{23} which we vary over their 3σ limits $2.435 \times 10^{-3}\,\text{eV}^2$ to $2.598 \times 10^{-3}\,\text{eV}^2$ and 40.1° to 51.7°, respectively [9].

We set $\sigma_\alpha = 0.25$ as the atmospheric flux normalization error, and $\sigma_\beta = 0.05$ as the zenith angle slope error [22]. The observed event number has an associated Poissonian uncertainty $\sigma^{\text{data}}_{ijk} = \sqrt{N^{\text{data}}_{ijk}}$. For IceCube, the event count takes the form

$$N^{\text{th}}_{ij} = \alpha\left[1 + \beta(0.5 + \cos(\theta_z^{reco})_i)\right] N_{ij}(\hat{\theta})\,, \tag{21}$$

with $N_{ij}(\hat{\theta})$ from Eq. 8. Here, we allow the event distribution to rotate around the median cosine-zenith of $\cos(\theta_z^{reco}) = -0.5$. The event index k is omitted since we only have track events for IceCube.

For DeepCore and PINGU, and the event count takes the form

$$N^{\text{th}}_{ijk} = \alpha\left[1 + \beta\cos(\theta_z^{reco})_i\right] N_{ijk}(\hat{\theta}) + \kappa N^{\mu_{atm}}_{ijk}\,, \tag{22}$$

with $N_{ijk}(\hat{\theta})$ from Eq. 12. $N^{\mu_{atm}}_{ijk}$ is the muon background, which is left to float freely in the DeepCore analysis. The detectors experience an uncorrelated systematic error, which comes from the muon background, i.e. events misclassified as muons from ν_μ interactions rather than from pion decay. For the DeepCore analysis, we will have to consider this background when calculating the events. For IceCube events,

Experiment	Best case	Baseline	Worst case
IceCube	5%	10%	15%
PINGU	0%	3%	5%

Table 5: Our definition of the best, baseline, and worst case scenarios considered in each experiment, modelled by $\sigma_{ijk}^{\text{syst}} = f\sqrt{N_{ijk}^{\text{data}}}$ with f from the table. We do not consider different DeepCore scenarios because her systematic error distribution is already provided in the data release [10].

we scan a higher energy range where the muon background can be neglected. For the PINGU events, the IceCube detector is expected to be able to act as a veto for this background. Thus, the error introduced from the muon background is expected by the collaboration to be negligible [5]. The background at PINGU can be considered negligible to first order [12], and we thus put $\kappa = 0$ when calculating the PINGU χ^2. For DeepCore and PINGU, the median cosine-zenith is $\cos(\theta_z^{reco}) = 0$, and we allow the event count to rotate around this point.

We treat the uncorrelated systematic uncertainties differently for each detector. For IceCube, we set $\sigma_{ij}^{\text{syst}} = f\sqrt{N_{ij}^{\text{data}}}$. We consider best, normal, and worst-case scenarios in IceCube using $f = 5\%$, 10%, and 15% respectively. For PINGU, we use the same form but instead use $f = 0\%$, 3%, and 5%. For DeepCore, we use the provided systematic error distribution which accounts for uncertainties in the finite MC statistics and the data-driven muon background estimate [10]. This is summarized in Table 5.

For the joint analysis, we follow the parameter goodness-of-fit prescription [23] and construct the joint χ^2 as

$$\chi^2_{\text{joint}} = \sum_{\text{exp}} \chi^2_{\text{exp}} - \chi^2_{\text{exp,min}} \tag{23}$$

with test statistic $\chi^2_{\text{joint,min}}$. The $\Delta\chi^2_{\text{joint}}$ is then $\Delta\chi^2_{\text{joint}} = \chi^2_{\text{joint}} - \chi^2_{\text{joint,min}}$.

8.2 Constraining the NSI parameters

We let each of the four NSI parameters considered assume a value, while keeping the other three fixed at zero. We consider the following ranges of values for each

parameter:

$$\begin{aligned} -0.07 \leq \epsilon_{\tau\tau} \leq 0.07 \\ -0.03 \leq \epsilon_{\mu\tau} \leq 0.03 \\ -0.3 \leq \epsilon_{e\mu} \leq 0.3 \\ -0.3 \leq \epsilon_{e\tau} \leq 0.3 \end{aligned} \tag{24}$$

After the oscillation parameters Δm^2_{31} and θ_{23} have been marginalized out, we plot $\Delta\chi^2$ for each of the four NSI parameters in Fig. 12. The results are shown in Fig. 13 and summarized in Tables 6 and 7. Each region is bounded by the best and worst-case scenario, as defined in Table 5, while the middle line is the baseline scenario. We again emphasize that no uncertainty scenarios are considered for DeepCore, since they already provided in the data release [10].

Comparing the PINGU and the DeepCore results in Fig. 12, we note that the best-fit for each NSI parameter for the PINGU experiment is expected to be zero. This is because the 'data' we generated during the PINGU simulations assume no NSI since they have yet to be observed in nature. This introduces a non-NSI bias in all joint analyses, which include PINGU since PINGU has stronger statistics than DeepCore and will thus pull the joint χ^2 towards $\epsilon = 0$. Moreover, we see that we can expect PINGU to be sensitive to systematic uncertainty, especially when constraining $\epsilon_{e\mu}$ and $\epsilon_{e\tau}$ from the negative side.

We compare our results to a similar analysis performed on the same DeepCore dataset in [24]. In that publication, the constraints found at 90% CL were

$$\begin{aligned} -0.055 < \epsilon_{\tau\tau} < 0.056 \\ -0.023 < \epsilon_{\mu\tau} < 0.016 \\ -0.21 < \epsilon_{e\mu} < 0.20 \\ -0.19 < \epsilon_{e\tau} < 0.20\,. \end{aligned} \tag{25}$$

Comparing 25 to our results from Table 6 at 90% CL, namely

$$\begin{aligned} -0.054 < \epsilon_{\tau\tau} < 0.067 \\ -0.029 < \epsilon_{\mu\tau} < 0.0070 \\ -0.12 < \epsilon_{e\mu} < 0.15 \\ -0.084 < \epsilon_{e\tau} < 0.15\,, \end{aligned} \tag{26}$$

we see that our results for $\epsilon_{e\mu}$, $\epsilon_{e\tau}$ are more stringent, while the results for $\epsilon_{\mu\tau}$ and $\epsilon_{\tau\tau}$ are similar but more lenient. It is worth noting that the results from [24] are have been obtained by including more systematic uncertainties, such as the

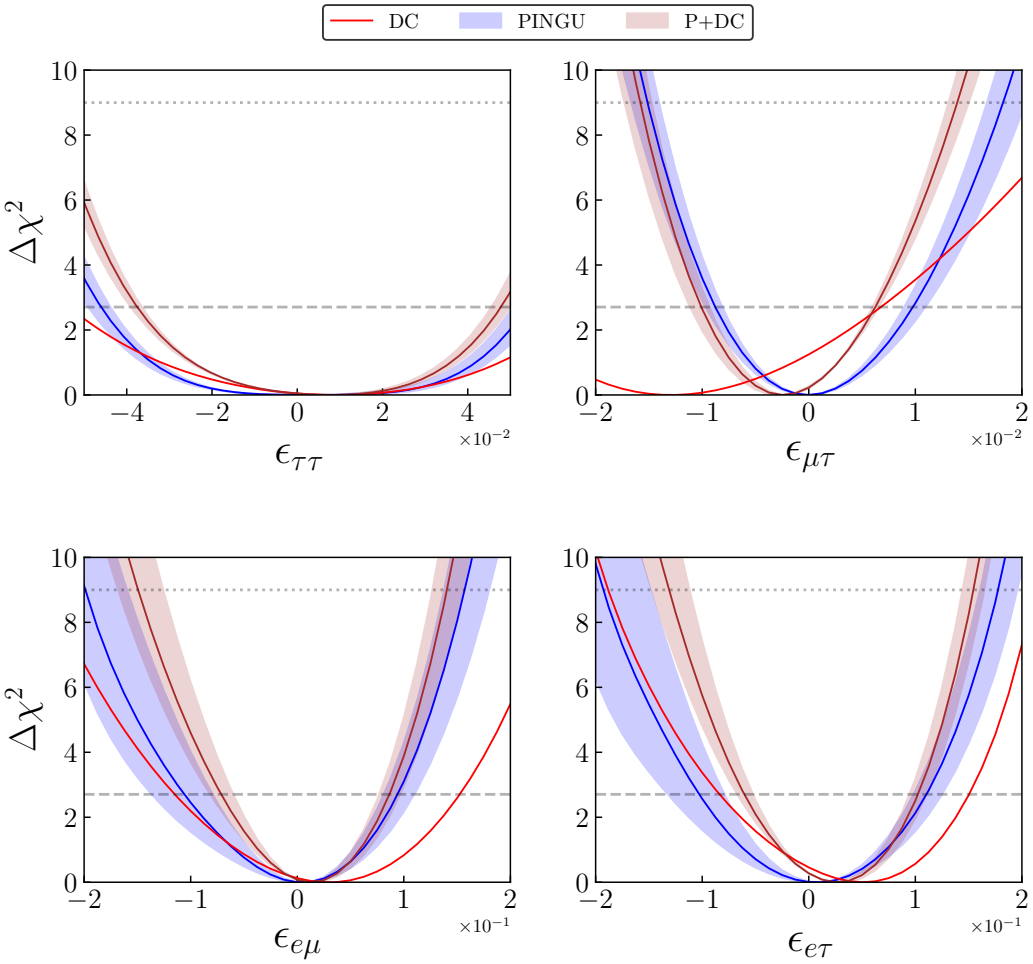

Figure 12: Confidence regions for PINGU and DeepCore scenarios listed in Table 5, with their joint $\Delta\chi^2$ in maroon. Δm^2_{31} and θ_{23} and have been marginalized out, and all other NSI parameters not shown in each panel are fixed to zero. IceCube tracks only reveal $\epsilon_{\mu\tau}$, and are displayed separately in Fig. 13. Dotted lines are the 90% and 3σ CL levels.

Parameter	Best 90% CL	Best 3σ
	IceCube	
$\epsilon_{\mu\tau}$	[-0.012, 0.011]	[-0.017, 0.016]
	DeepCore	
$\epsilon_{\tau\tau}$	[-0.054, 0.067]	[-0.089, 0.10]
$\epsilon_{\mu\tau}$	[-0.029, 0.0070]	[-0.041, 0.026]
$\epsilon_{e\mu}$	[-0.12, 0.15]	[-0.23, 0.24]
$\epsilon_{e\tau}$	[-0.084, 0.15]	[-0.19, 0.21]
	IceCube + DeepCore	
$\epsilon_{\mu\tau}$	[-0.013, 0.0070]	[-0.017, 0.013]

Parameter	Baseline 90% CL	Baseline 3σ
	IceCube	
$\epsilon_{\mu\tau}$	[-0.015, 0.014]	[-0.022, 0.021]
	DeepCore	
$\epsilon_{\tau\tau}$	[-0.054, 0.067]	[-0.089, 0.10]
$\epsilon_{\mu\tau}$	[-0.029, 0.0070]	[-0.041, 0.026]
$\epsilon_{e\mu}$	[-0.12, 0.15]	[-0.23, 0.24]
$\epsilon_{e\tau}$	[-0.084, 0.15]	[-0.19, 0.21]
	IceCube + DeepCore	
$\epsilon_{\mu\tau}$	[-0.016, 0.0070]	[-0.022, 0.016]

Parameter	Worst 90% CL	Worst 3σ
	IceCube	
$\epsilon_{\mu\tau}$	[-0.018, 0.017]	[-0.025, 0.024]
	DeepCore	
$\epsilon_{\tau\tau}$	[-0.054, 0.067]	[-0.089, 0.10]
$\epsilon_{\mu\tau}$	[-0.029, 0.0070]	[-0.041, 0.026]
$\epsilon_{e\mu}$	[-0.11, 0.15]	[-0.23, 0.24]
$\epsilon_{e\tau}$	[-0.084, 0.15]	[-0.188, 0.212]
	IceCube + DeepCore	
$\epsilon_{\mu\tau}$	[-0.018, 0.0070]	[-0.024, 0.018]

Table 6: IceCube and DeepCore results from the $\Delta\chi^2$ in Fig. 13. Δm^2_{31} and θ_{23} have been marginalized out, and all other NSI parameters other than the one shown for each row are set to zero. Best, baseline, and worst refer to the systematic uncertainty scenarios considered as in Table 5.

Parameter	Best 90% CL	Best 3σ
	PINGU	
$\epsilon_{\tau\tau}$	[-0.044, 0.051]	[-0.062, 0.069]
$\epsilon_{\mu\tau}$	[-0.008, 0.009]	[-0.014, 0.017]
$\epsilon_{e\mu}$	[-0.079, 0.081]	[-0.16, 0.138]
$\epsilon_{e\tau}$	[-0.079, 0.098]	[-0.148, 0.161]
	DeepCore + PINGU	
$\epsilon_{\tau\tau}$	[-0.036, 0.046]	[-0.056, 0.064]
$\epsilon_{\mu\tau}$	[-0.0090, 0.0060]	[-0.015, 0.013]
$\epsilon_{e\mu}$	[-0.060, 0.077]	[-0.13, 0.13]
$\epsilon_{e\tau}$	[-0.052, 0.095]	[-0.11, 0.14]
	IceCube + DeepCore + PINGU	
$\epsilon_{\mu\tau}$	[-0.0080, 0.0050]	[-0.012, 0.011]
Parameter	Baseline 90% CL	Baseline 3σ
	PINGU	
$\epsilon_{\tau\tau}$	[-0.046, 0.054]	[-0.065, 0.073]
$\epsilon_{\mu\tau}$	[-0.0090, 0.010]	[-0.015, 0.018]
$\epsilon_{e\mu}$	[-0.11, 0.094]	[-0.20, 0.16]
$\epsilon_{e\tau}$	[-0.10, 0.11]	[-0.19, 0.18]
	DeepCore + PINGU	
$\epsilon_{\tau\tau}$	[-0.038, 0.048]	[-0.058, 0.067]
$\epsilon_{\mu\tau}$	[-0.010, 0.0060]	[-0.016, 0.014]
$\epsilon_{e\mu}$	[-0.071, 0.086]	[-0.15, 0.14]
$\epsilon_{e\tau}$	[-0.061, 0.10]	[-0.13, 0.16]
	IceCube + DeepCore + PINGU	
$\epsilon_{\mu\tau}$	[-0.009, 0.0060]	[-0.014, 0.012]
Parameter	Worst 90% CL	Worst 3σ
	PINGU	
$\epsilon_{\tau\tau}$	[-0.049, 0.057]	[-0.07, 0.078]
$\epsilon_{\mu\tau}$	[-0.01, 0.011]	[-0.017, 0.02]
$\epsilon_{e\mu}$	[-0.137, 0.11]	[-0.228, 0.18]
$\epsilon_{e\tau}$	[-0.132, 0.125]	[-0.226, 0.196]
	DeepCore + PINGU	
$\epsilon_{\tau\tau}$	[-0.039, 0.050]	[-0.060, 0.070]
$\epsilon_{\mu\tau}$	[-0.011, 0.0070]	[-0.017, 0.015]
$\epsilon_{e\mu}$	[-0.082, 0.097]	[-0.168, 0.16]
$\epsilon_{e\tau}$	[-0.067, 0.11]	[-0.15, 0.17]
	IceCube + DeepCore + PINGU	
$\epsilon_{\mu\tau}$	[-0.010, 0.0060]	[-0.016, 0.013]

Table 7: PINGU and joint results from the $\Delta\chi^2$ in Fig. 12. Δm^2_{31} and $\theta[23]$ have been marginalized out, and all other NSI parameters other than the one shown for each row are set to zero. Best, baseline, and worst refer to the systematic uncertainty scenarios considered as in Table 5.

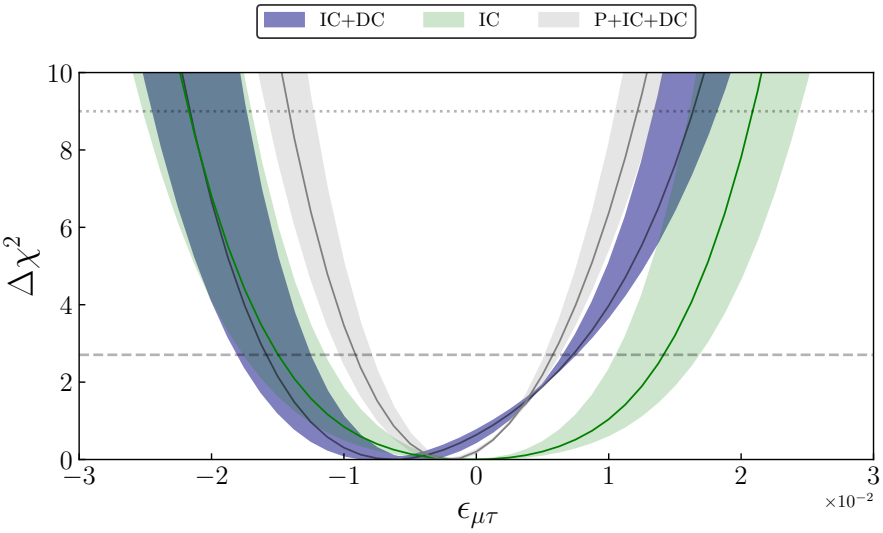

Figure 13: $\epsilon_{\mu\tau}$ $\Delta\chi^2$ regions for scenarios as defined in Table 5. Δm^2_{31} and θ_{23} and have been marginalized out, and all other NSI parameters other than $\epsilon_{\mu\tau}$ are fixed to zero. Dotted lines are the 90% and 3σ CL levels. The zones contain the three uncertainty scenarios considered, and we see that the inclusion of PINGU is expected to drastically make the bound on $\epsilon_{\mu\tau}$ more stringent.

	Best fit		
Parameter	Δm^2_{31}	θ_{23}	ϵ
	DeepCore		
$\epsilon_{\tau\tau}$	2.435	47.84	0.0125
$\epsilon_{\mu\tau}$	2.435	43.97	-0.005
$\epsilon_{e\mu}$	2.435	43.97	0
$\epsilon_{e\tau}$	2.435	43.97	0.05
	IceCube		
$\epsilon_{\mu\tau}$	2.435	51.70	0
	IceCube + DeepCore		
$\epsilon_{\mu\tau}$	2.517	43.97	-0.01

Table 8: Best fit points for Δm^2_{31} and θ_{23} are given in units of 10^{-3}eV^2 and degrees, respectively.

spectral index, hadron production, and baryon resonance. However, the overall flux normalization in [24] is 20%, while we opted for a slightly higher figure of 25%, which could compensate for the exclusion of the statistical uncertainties mentioned.

Using the baseline case of 3% systematic uncertainty at 90% CL, we find from Table 7, that our predictions for the proposed PINGU detector are

$$\begin{aligned} -0.049 &< \epsilon_{\tau\tau} < 0.057 \\ -0.010 &< \epsilon_{\mu\tau} < 0.011 \\ -0.137 &< \epsilon_{e\mu} < 0.11 \\ -0.132 &< \epsilon_{e\tau} < 0.125\,, \end{aligned} \tag{27}$$

which displays an improvement over the DeepCore results in Eq. 26, except for $\epsilon_{e\tau}$ which is worse.

Finally, the joint results for $\epsilon_{\mu\tau}$ using IceCube and DeepCore from 7 at 90% CL are

$$-0.016 < \epsilon_{\mu\tau} < 0.0070\,, \tag{28}$$

and when combining IceCube, DeepCore, and PINGU, the 90% CL constraint on $\epsilon_{\mu\tau}$ in our baseline scenario is predicted to be

$$-0.010 < \epsilon_{\mu\tau} < 0.0060\,, \tag{29}$$

which is more stringent for $\epsilon_{\mu\tau} > 0$ than the result in [25].

We plot the event pull $(N_{NSI} - N_{SI})/\sqrt{N_{SI}}$ where $N_{(N)SI}$ are the numbers of expected events assuming (non-)standard interactions in Fig. 14. This gives the normalized difference in the number of expected events at the detector and illustrates the expected sensitivity of DeepCore for the NSI parameters.

Now we will compare the probability plots with the final event counts in DeepCore. It is not enough to only study the effect at probability level, since that is in true quantities. Since the detector data comes in reconstructed quantities, it might be the case that a feature at probability level gets averaged out in the reconstruction, and not showing up at all in the data. In general, features showing at probability level are can be averaged out at reconstruction if they occur in the rapidly oscillating part of single-digit GeV energies.

The top right panel shows a surplus of DeepCore track events at 20 GeV to 30 GeV for through-going neutrinos when we turn on $\epsilon_{\tau\tau}$. This is what we expected from the bottom right panel in Fig. 8, where we saw that we had an increase in $\bar{\nu}_\mu$ survival probability at 20 GeV to 40 GeV.

The third right panel shows the expected event pull for $\epsilon_{e\mu}$. Comparing with the probabilities in Fig. 9, we see that the surplus of the $\bar{\nu}_\mu$ survival in the 20 GeV

to 30 GeV and the deficit above 40 GeV is intact, while the 10 GeV ν_μ deficit is completely averaged out.

There is no reason for us to assume that only one NSI parameter exists in Nature, unless we impose a symmetry on the gauge group which generates NSI. For example, the matter potential matrix in our Hamiltonian from Eq. (**??**) is diagonal since the interaction Lagrangian respects lepton flavor conservation. So ideally, we would simulate a grid where all NSI parameters are allowed to vary, but this is not feasible. Thus, we take we set $\epsilon_{\tau\tau} = 0$ and let $\epsilon_{\mu\tau}, \epsilon_{e\mu}, \epsilon_{e\tau}$ vary, along with Δm^2_{31} and θ_{23}. We let $\epsilon_{\tau\tau} = 0$ because we saw that it did not influence the other parameters. We then marginalize out the standard oscillation parameters and one of the NSI parameters and plot the remaining two in Fig. 15. We see that the pairs $\epsilon_{e\mu} - \epsilon_{\mu\tau}$ and $\epsilon_{e\tau} - \epsilon_{\mu\tau}$ are symmetrical. Hence, we can see that no relationship exists between them. With $\epsilon_{e\tau} - \epsilon_{e\mu}$, however, the contours are assuming a different shape. The contour allows positive values of $\epsilon_{e\tau}$ and $\epsilon_{e\mu}$ to a greater degree than mixed or negative values. Thus, we can draw the conclusion that, given $\epsilon_{\tau\tau} = 0$, PINGU might expect to observe that $\epsilon_{e\mu}$ and $\epsilon_{\mu\tau}$ are anti-correlated while we expect no significant correlation to be be seen between the pairs $\epsilon_{\mu\tau} - \epsilon_{e\mu}$, and $\epsilon_{\mu\tau} - \epsilon_{e\tau}$. This is consistent with our observation of the effect of these parameters on $P_{\mu e}$ in Fig. 11, from which we saw that $\epsilon_{e\mu}$ and $\epsilon_{e\tau}$ strongly affect $P_{\mu e}$ for single-digit GeV energies.

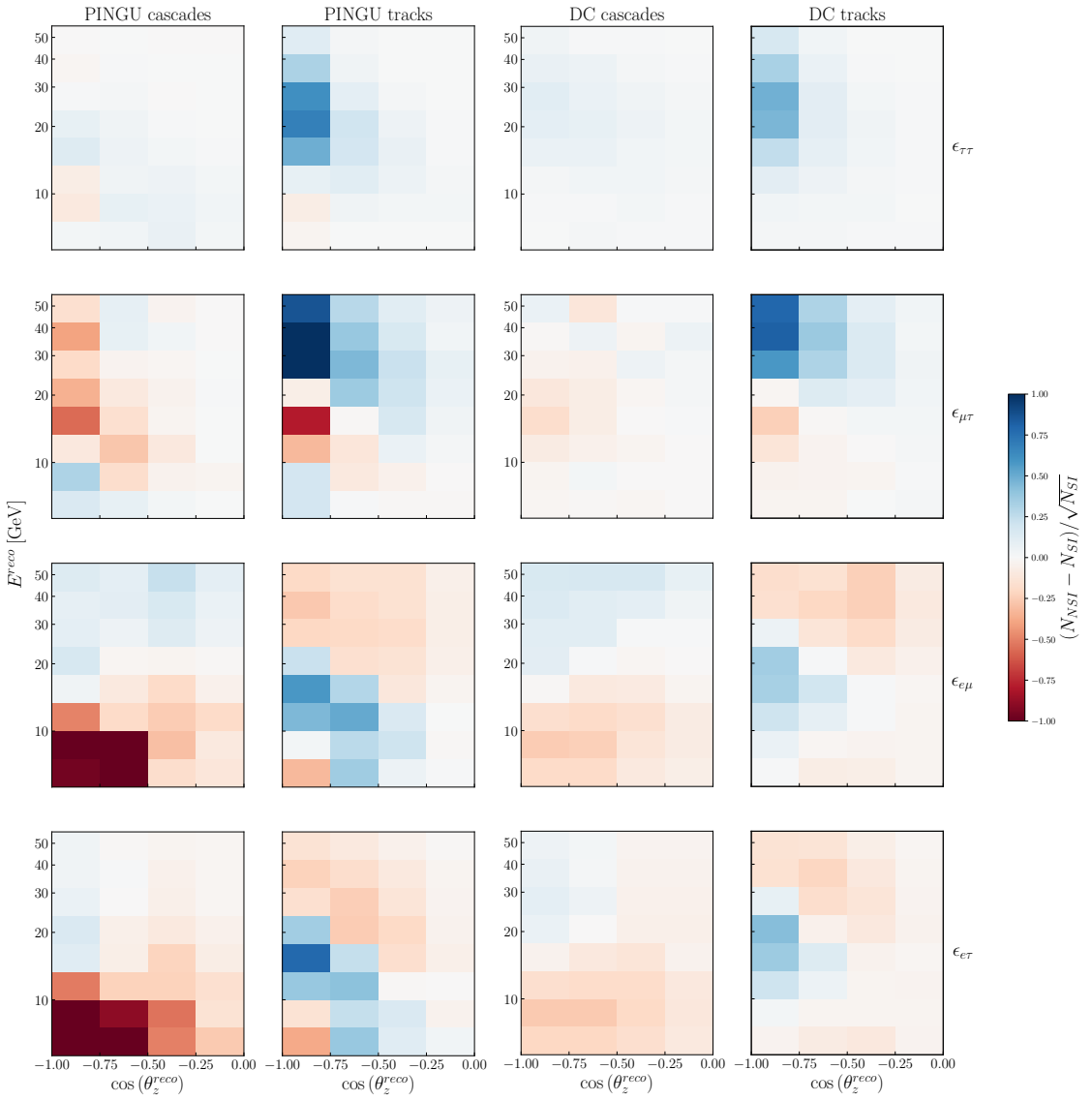

(a) PINGU (b) DeepCore

Figure 14: Expected pulls of the form $(N_{NSI}-N_{SI})/\sqrt{N_{SI}}$ for PINGU and DeepCore after 3 years of data. Each row has only one NSI non-zero parameter, with the first row having $\epsilon_{\tau\tau} = -0.07$, second $\epsilon_{\mu\tau} = -0.03$, third $\epsilon_{e\mu} = -0.3$, and fourth $\epsilon_{e\tau} = -0.3$. We clearly see the increased statistics of the PINGU detector, especially in cascade events. The low values of $\epsilon_{\tau\tau}$ and $\epsilon_{\mu\tau}$ produce a weak pull in DeepCore, while PINGU can be expected to observe multiple regions of strong pulls for $\epsilon_{\mu\tau}$, $\epsilon_{e\mu}$, and $\epsilon_{e\tau}$.

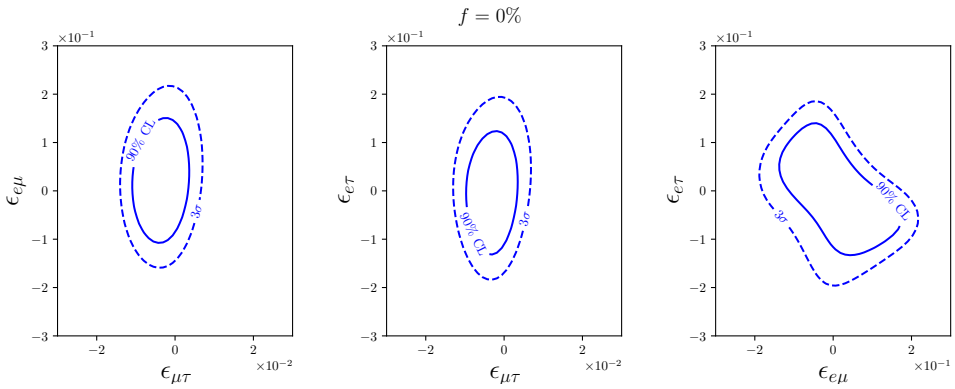

Figure 15: Allowed regions for some of the NSI parameters after three years of PINGU data, assuming no uncorrelated systematic error. All plots are made with $\epsilon_{\tau\tau} = 0$. The two standard oscillation parameters Δm^2_{31} and θ_{23} along with the one NSI parameter not shown have been marginalized out. We observe an anti-correlation between $\epsilon_{e\mu}$ and $\epsilon_{e\tau}$, consistent with our observation of the effect of these parameters on $P_{\mu e}$ in Fig. 11. The values of the standard oscillation parameters are taken from NuFit [9].

Conclusion

We introduced Non-Standard Interactions (NSI) in Sec. 7 as a possible example of new physics beyond the Standard Model. We then studied the effects of NSI on the neutrino oscillation probabilities and saw that NSI effects other than those stemming from $\epsilon_{\mu\tau}$ are not apparent in the TeV region. Moreover, we saw in $P_{\mu e}$ that we could expect a correlation between $\epsilon_{e\mu}$ and $\epsilon_{e\tau}$ in the single-digit GeV range. We also saw that $\epsilon_{\mu\tau}$ effects were visible on probability level in both the GeV and TeV regions.

We simulated the 86 string IceCube detector with track events, explained in Sec. 4. In Sec. 8, we studied the NSI parameter $\epsilon_{\mu\tau}$ and its effect events captured by IceCube. Using a χ^2 test, we found that the bound from IceCube on $\epsilon_{\mu\tau}$ at 90 % confidence level was

$$-0.015 < \epsilon_{\mu\tau} < 0.014 \quad (90\% \text{ CL}) \tag{30}$$

for our 'baseline' case of 15% uncorrelated systematic uncertainty.

In Sec. 5, we moved on and explained our method of simulating a second detector, DeepCore. Armed with simulations possible for this detector, we then continued to explore the possibility of NSI, this time including both track and cascade events and a lower energy region. Using the χ^2 test defined in Eq. 20 and after marginalizing Δm^2_{31} and θ_{23} out, we found the following constraints on the NSI parameters at 90% confidence level:

$$\begin{aligned} -0.054 &< \epsilon_{\tau\tau} < 0.067 \\ -0.029 &< \epsilon_{\mu\tau} < 0.0070 \\ -0.12 &< \epsilon_{e\mu} < 0.15 \\ -0.084 &< \epsilon_{e\tau} < 0.15 \quad \text{(all at 90\% CL)}\,. \end{aligned} \tag{31}$$

We compared these constraints to literature and found that the bounds for $\epsilon_{e\mu}$ and $\epsilon_{e\tau}$ were more stringent than those obtained in [24]. Then, we did a joint χ^2 test using simulated events from both IceCube and DeepCore. At 90% confidence level, the bound of $\epsilon_{\mu\tau}$ improved to

$$-0.016 < \epsilon_{\mu\tau} < 0.0070 \quad (90\% \text{ CL})\,. \tag{32}$$

In Sec. 6 we described our method of simulating a proposed upgrade to the IceCube array: PINGU. Since PINGU is not yet live, we produced data for it assuming a standard 3 neutrino hypothesis with parameters from [9]. After a χ^2 analysis, we

obtained the following constrains on the NSI parameters at 90% confidence level:

$$\begin{aligned} &-0.049 < \epsilon_{\tau\tau} < 0.057 \\ &-0.010 < \epsilon_{\mu\tau} < 0.011 \\ &-0.137 < \epsilon_{e\mu} < 0.11 \\ &-0.132 < \epsilon_{e\tau} < 0.125 \quad \text{(all at 90\% CL)}\,. \end{aligned} \tag{33}$$

After that, we did a joint χ^2 analysis combining IceCube, DeepCore and simulated PINGU events to further constrict $\epsilon_{\mu\tau}$. The bound at 90% confidence level obtained was

$$-0.010 < \epsilon_{\mu\tau} < 0.0060\,. \quad \text{(90\% CL)} \tag{34}$$

We were then able to draw the conclusion that we expect PINGU to successfully be able to observe the impact of NSI. Moreover, a joint analysis between PINGU and at least one of the other detectors under the IceCube collaboration will be able to constrain the parameters even further. We saw that can expect PINGU to be more sensitive to NSI effects than DeepCore. We were also able to see that when constraining $\epsilon_{e\mu}$ and $\epsilon_{e\tau}$ from the negative side, we can expect the result to be highly dependent on the systematic uncertainty of PINGU.

Finally, we simulated the event count in PINGU, allowing $\epsilon_{\mu\tau}$, $\epsilon_{e\mu}$, and $\epsilon_{e\tau}$ to vary, but setting $\epsilon_{\tau\tau} = 0$. After and marginalizing out Δm^2_{31}, θ_{23}, and $\epsilon_{\mu\tau}$, we saw that the effect of $\epsilon_{e\mu}$ and $\epsilon_{e\tau}$ on $P_{\mu e}$ had indeed propagated through to the event count, manifesting as an anti-correlation between the $\epsilon_{e\mu}$ and $\epsilon_{e\tau}$ at both 90% and 3σ confidence levels. No other pair of NSI parameters were observed to have a significant correlation.

References

[1] M. Honda, HKKM2014 flux table one year average.
URL http://www.icrr.u-tokyo.ac.jp/~mhonda/nflx2014/index.html

[2] M. Honda et al., Atmospheric neutrino flux calculation using the NRLMSISE-00 atmospheric model 92 (2) 023004. doi:10.1103/PhysRevD.92.023004.

[3] The IceCube Collaboration, Measurement of atmospheric tau neutrino appearance with IceCube DeepCore 99 (3) 032007. doi:10.1103/PhysRevD.99.032007.

[4] C. Weaver, Evidence for Astrophysical Muon Neutrinos from the Northern Sky.

[5] The IceCube Gen2 Collaboration, Letter of Intent: The Precision IceCube Next Generation Upgrade (PINGU). arXiv:1401.2046.

[6] The IceCube Collaboration, All-sky point-source IceCube data: Years 2010-2012. doi:10.21234/B4F04V.

[7] The IceCube Collaboration, Search for sterile neutrinos with one year of IceCube data.
URL https://icecube.wisc.edu/data-releases/2016/06/search-for-sterile-neutrinos-with-one-year-of-icecube-data/

[8] The IceCube Collaboration et al., Searching for eV-scale sterile neutrinos with eight years of atmospheric neutrinos at the IceCube Neutrino Telescope 102 (5) 052009. doi:10.1103/PhysRevD.102.052009.

[9] I. Esteban et al., The fate of hints: Updated global analysis of three-flavor neutrino oscillations 2020 (9) 178. doi:10.1007/JHEP09(2020)178.

[10] The IceCube Collaboration, Three-year high-statistics neutrino oscillation samples. doi:10.21234/ac23-ra43.

[11] The IceCube Collaboration, Measurement of Atmospheric Neutrino Oscillations at 6–56 GeV with IceCube DeepCore 120 (7) 071801. doi:10.1103/PhysRevLett.120.071801.

[12] The IceCube Collaboration, IceCube Upgrade Neutrino Monte Carlo Simulation. doi:10.21234/qfz1-yh02.

[13] M. B. Gavela et al., Minimal Flavour Seesaw Models 2009 (09) 038–038. arXiv:0906.1461, doi:10.1088/1126-6708/2009/09/038.

[14] J. Salvado et al., Non-standard interactions with high-energy atmospheric neutrinos at IceCube 2017 (1) 141. arXiv:1609.03450, doi:10.1007/JHEP01(2017)141.

[15] Y. Farzan and M. Tortola, Neutrino oscillations and Non-Standard Interactions. arXiv:1710.09360.

[16] T. Ohlsson, Status of non-standard neutrino interactions 76 (4) 044201. arXiv:1209.2710, doi:10.1088/0034-4885/76/4/044201.

[17] P. Coloma et al., A COHERENT enlightenment of the neutrino Dark Side 96 (11) 115007. arXiv:1708.02899, doi:10.1103/PhysRevD.96.115007.

[18] The IceCube Collaboration, All-flavor constraints on nonstandard neutrino interactions and generalized matter potential with three years of IceCube DeepCore data. arXiv:2106.07755.

[19] A. Esmaili and A. Y. Smirnov, Probing Non-Standard Interaction of Neutrinos with IceCube and DeepCore 2013 (6) 26. arXiv:1304.1042, doi:10.1007/JHEP06(2013)026.

[20] S. Choubey and T. Ohlsson, Bounds on Non-Standard Neutrino Interactions Using PINGU 739 357–364. doi:10.1016/j.physletb.2014.11.010.

[21] T. Ohlsson et al., Effects of nonstandard neutrino interactions at PINGU 88 (1) 013001. doi:10.1103/PhysRevD.88.013001.

[22] M. Honda et al., Calculation of atmospheric neutrino flux using the interaction model calibrated with atmospheric muon data.doi:10.1103/PhysRevD.75.043006.

[23] M. Maltoni and T. Schwetz, Testing the statistical compatibility of independent data sets 68 (3) 033020. arXiv:hep-ph/0304176, doi:10.1103/PhysRevD.68.033020.

[24] S. Demidov, Bounds on non-standard interactions of neutrinos from IceCube DeepCore data 2020 (3) 105. doi:10.1007/JHEP03(2020)105.

[25] The IceCube Collaboration, Search for nonstandard neutrino interactions with IceCube DeepCore 97 (7) 072009. doi:10.1103/PhysRevD.97.072009.